Journal of Nanofluids
Vol. 10, pp. 118–127, 2021
(www.aspbs.com/jon)

ARTICLE

Zero Mass Flux Dependent on Radiative Magnetohydrodynamics Carreau Nanofluid Over a Radially Surface with Temperature Jump and Slip Flow: A Hybrid Nanofluid Analysis

Amit Parmar[1,*], Rakesh Choudhary[2], and Krishna Agrawal[1]

[1] *Poornima University, Jaipur 303905, Rajasthan, India*
[2] *Bhartiya Skill Development University Jaipur, 302042, Rajasthan, India*

The present study explores the slip flow and heat transfer induced by a radially surface with MHD Carreau nanofluid. In addition, the effects of temperature jump, non-linear radiation and the dependent zero mass flux also taken into account. This study also considers the cross-diffusion effect on temperature and concentration governing profiles. Appropriate transformations are engaged in order to acquire nonlinear differential equations (ODEs) from the partial differential system, their solutions are obtained by Runge-Kutta 4th order with shooting scheme in MATLAB. The impact of pertinent flow parameters such as first and second order velocity slip parameter, temperature jump, magnetic parameter, heat source, radiation parameter, melting surface parameter, temperature ratio parameter on dimensionless velocity, temperature and concentration profiles achieved graphically as well as local skin friction, Nusselt number and Sherwood number are demonstrated in the form of Table. first order velocity slip parameter ($slip_1$) on f', θ and ϕ profile fields. With an increment in the velocity slip first order parameter ($slip_1$) we have perceived a fall in the momentum boundary layer and concentration profiles and a growth in the fluid temperature field.

KEYWORDS: Radially Surface, Carreau Nanofluid, MHD, Second Order Slip, Non-Linear Radiation, Zero Mass Flux.

1. INTRODUCTION

For MHD, the issue of boundary layer flow Carreau nanofluid for heat and mass transfer to calculate the combined effect of second order velocity slip with zero mass flux over a malting radially surface plays a significant role in the construction of many durable machinery in the industrial industries. Many researchers are interested in studying melting surfaces because of their uses in engineering and domains like extrusion, hot rolling melt-spinning, glass-fiber processing, wire drawing, bath cooling of a large metallic layer, production of plastic and rubber mats, and so on.

Khan et al.[1] computational analysis of the unsteady Falkner-Skan flow of Carreau nanofluid with heat generation/absorption and melting phenomenon, taking into consideration the above applications. Azam et al.[2] studied the unsteady flow of Carreau nanofluid over an expanding/contracting cylinder within the presence of MHD. Khan et al.[3–4] investigated the unsteady MHD heat and mass flow processes caused by an absorbent stretching surface within the presence of Carreau nanofluid flow. The unsteady MHD flow of Carreau nanofluid past a radially extending layer was studied by Khan et al.[5] The results of MHD Carreau fluid on the incidence of Newtonian heating and slip flow were studied by Hayat et al.[6–7] Furthermore, some interesting investigations on nanofluids can be found such as Waqas et al.,[8] Sulochana et al.[9] Ramzan et al.,[10–12] Rahman et al.,[13–14] Upreti et al.,[15] Turkyilmazoglu,[16] Goyal and Bhargava,[17] Khan et al.,[18] Jain et al.,[19–21] Rahman[22] Megahed,[23] Gorla et al.,[24] Makinde et al.,[25] Azam et al.[26] and Ramzan et al.[27]

No doubt, heat transportation with non-linear radiation is prominent explicitly for the nanofluids in spite of adequate velocities. It converts energy (kinetic to internal) i.e., fluid warming due to viscosity and accordingly intensifications the liquid movement. The concept of nanofluids has fascinated the continual thoughtfulness of academics. It's due to the circumstance that an emergent mixture which contains of solid particles scattered in conservative heat transfer base fluids. Base fluids (such as water, oil

*Author to whom correspondence should be addressed.
Email: amit.198631@gmail.com
Received: 25 April 2021
Accepted: 2 May 2021

 2169-432X/2021/10/118/010 doi:10.1166/jon.2021.1773

and ethanediol, etc.) are poor conductors of warmth and thus they need great role on the speed of warmth transfer among the medium and surface of warmth transfer. Consequently, considerable methods are trusted on enrich the thermal conductivity of those fluids by swinging nanoparticles in fluids. within the industries, Nanotechnology could also be utilized because of its numerous applications and features. The Physical and chemical characteristics of its materials in terms of the dimensions of nanometer make the technology more adaptable. the primary analysis of nanofluids was given by Choi.[28]

Taking into consideration to the present point, numerous researchers like Muhammad et al.[29] investigated the mathematical modeling and analysis of non-linear radiative MHD Carreau nanofluid flow within the presence of warmth generation. Irfan et al.[30] studied the impacts of Arrhenius energy of activation in nonlinear mixed convection subject to chemically reactive radiative 3D Carreau nanofluid flow. A numerical analysis of chemically reactive nanofluid Carreau flow past a convectively nonlinear stretching surface was studied by Eid et al.[31]

Several Researchers[32–62] investigation of Various non-Newtonian and Newtonian fluid flow over various physical parameter effect on various boundary conditions and various surfaces.

The above mentioned researches observed that Carreau nanofluids liquids aren't yet scrutinized through nonlinear radiation with temperature jump and zero mass flux aspect. Therefore, our foremost attention here is to endeavor further during this regime by considering MHD Carreau nano-fluid mathematical model particularizes shear (thinning, thickening) properties. The Buongiorno model for nanofluids is measured for modeling.

2. MATHEMATICAL FORMULATION

Consider the 2D incompressible nano-Carreau fluid for momentum, temperature and mass transfer of *ax* symmetric. An identical field of force that encompasses a strength B_0 is executed in z-direction subject to absence of an induced field. The surface is extended radially with stretching velocity $u_w(r) = ar$, in where r is that the distance from the origin and a could be a non-negative constant.

The surface that corresponds with the plane $z = 0$ and fluid is limited to $z \geq 0$. The structure of cylindrical polar coordinate (r, θ, z) is chosen for numerical analysis (see Fig. 1). In fact, the zero-mass flux state is also introduced at the surface. The undeviating temperature at the surface is T_w and far away from the surface is T_∞ such that $T_w > T_\infty$. At the surface of sheet, the nanoparticles concentration is restricted by

$$D_B \frac{\partial C}{\partial z} + \frac{D_T}{T_\infty}\frac{\partial T}{\partial z} = 0$$

and far from the surface i.e., the ambient concentration is taken to be C_∞ which is constant. Where u and w

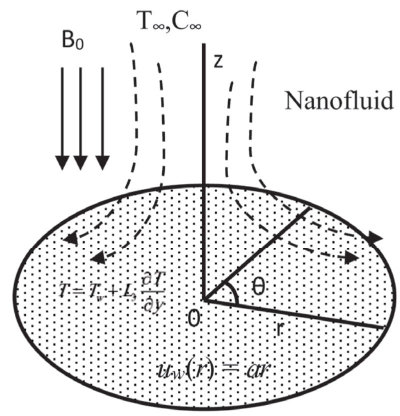

Fig. 1. Schematic diagram of the problem.

represent the velocities of r and z directions, T; temperature distribution, C; nanoparticles volume fraction, D_B and D_T are the "Brownian motion and thermophoresis" diffusion coefficients, individually. Moreover, Q; heat generation/absorption coefficient, k_n; rate of chemical reaction and q_r ; Rosseland's radiation flux.

The basic equations for an incompressible fluid representing mass, linear momentum, energy and concentration without body forces are given as below:

The continuity, momentum, energy and mass governing equations.

$$\frac{\partial u}{\partial r} + \frac{\partial v}{\partial z} = 0 \tag{1}$$

$$\begin{aligned} u\frac{\partial u}{\partial r} + w\frac{\partial u}{\partial z} &= v\frac{\partial^2 u}{\partial z^2}\left(1+\Gamma^2\left(\frac{\partial u}{\partial z}\right)^2\right)^{(n-1)/2} \\ &\quad + v(n-1)\Gamma^2\frac{\partial^2 u}{\partial z^2}\left(\frac{\partial u}{\partial z}\right)^2 \\ &\quad \times\left(1+\Gamma^2\left(\frac{\partial u}{\partial z}\right)^2\right)^{(n-3)/2} \\ &\quad - \frac{\sigma B_0^2}{\rho}u \end{aligned} \tag{2}$$

$$\begin{aligned} u\frac{\partial T}{\partial r} + w\frac{\partial T}{\partial z} &= \alpha\frac{\partial^2 T}{\partial z^2} - \frac{1}{\rho C_p}\frac{\partial q_r}{\partial z} \\ &\quad + \tau\left[D_B\frac{\partial C}{\partial z}\frac{\partial T}{\partial z} + \frac{D_T}{T_\infty}\left(\frac{\partial T}{\partial z}\right)^2\right] \\ &\quad + \frac{Q}{\rho C_f}(T - T_\infty) \end{aligned} \tag{3}$$

$$u\frac{\partial C}{\partial r} + w\frac{\partial C}{\partial z} = D_B\frac{\partial^2 C}{\partial z^2} + \frac{D_T}{T_\infty}\frac{\partial^2 T}{\partial z^2} - k_n(C - C_\infty) \tag{4}$$

Subject to boundary conditions[23, 24]

$$u = u_w(r) + L_1\frac{\partial u}{\partial z} + L_2\frac{\partial^2 u}{\partial z^2},$$
$$w = \frac{k}{\rho\left[\beta + c_s(T_m - T_0)\right]}\frac{\partial T}{\partial z},$$
$$T = T_w + L_3\frac{\partial T}{\partial y}, \quad D_B\frac{\partial C}{\partial z} + \frac{D_T}{T_\infty}\frac{\partial T}{\partial z} = 0, \quad \text{at} \quad z = 0$$
$$u \to 0, \quad T \to T_\infty, \quad C \to C_\infty \quad \text{at} \quad z \to \infty \tag{5}$$

Following Rosseland approximation q_r, the radiation heat flux is given (see Gorla et al. [24]).

$$q_r = -\left(\frac{4\sigma}{3k^*}\right)\frac{\partial T^4}{\partial y} = -\left(\frac{16\sigma}{3k^*}\right)T^3\frac{\partial T}{\partial y}$$

3. SOLUTION

The similarity solutions of Eqs. (1)–(4), are obtained using the given similarity transformations

$$u = ar\,f'(\eta), \quad w = -2\sqrt{av}f(\eta), \quad \eta = z\sqrt{\frac{a}{v}},$$
$$\theta(\eta) = \frac{T - T_\infty}{T_w - T_\infty} \quad \text{and} \quad \phi = \frac{C - C_\infty}{C_\infty} \tag{6}$$

Equations (2)–(5) and using Eq. (6) thus reduces to the following non-dimensional form

$$\left\{1 + n\,We^2\,(f'')^2\right\}\left\{1 + We^2\,(f'')^2\right\}^{(n-3)/2} f''' - f'^2 + 2f''f - M\,f' = 0 \tag{7}$$

$$\theta''\left(1 + \frac{4}{3}R\left((\theta_w - 1)\theta + 1\right)^3\right) + 4R(\theta_w - 1)\theta'^2((\theta_w - 1) \times \theta + 1)^2 + \Pr\left(2f\theta' + N_b\theta'\phi' + N_t\theta'^2 + \delta\theta\right) = 0 \tag{8}$$

$$\phi'' - Sc\,(K_n\phi - f\phi') + \frac{N_t}{N_b}\theta'' = 0 \tag{9}$$

Boundary conditions Eq. (11) reduces to:

$$\eta = 0: \quad f'(\eta) = 1 + Slip_1 f''(\eta) + Slip_2 f'''(\eta),$$
$$Prf(\eta) + Me\,\theta'(\eta) = 0;$$
$$\theta(\eta) = 1 + Slip_T\theta'(\eta),$$
$$N_b\phi'(\eta) + N_t\theta'(\eta) = 0$$
$$\eta \to \infty: \quad f'(\eta) \to 0, \quad \theta(\eta) \to 0, \quad \phi(\eta) \to 0 \tag{10}$$

Where, $We = (\Gamma^2 a^3 r^2)/\nu$; Weissenberg number, $Slip_1 = L_1\sqrt{a/\nu}$; first order slip velocity $Slip_2 = L_2(a/\nu)$; second order slip parameter $Slip_T = L_3\sqrt{(a/\nu)}$, temperature slip parameter, $R = (4\sigma T_\infty^3)/(k_\infty k*)$; Radiation parameter, $k*$; thermal radiation parameter, $M = (\sigma B_0^2)/(a\rho)$: Magnetic field parameter, $K_n = (k_n/a)(C_w - C_\infty)^{n-1}$: chemical reaction parameter, $\delta = Q/(a\,(\rho c)_f)$; $\delta < 0$ refers to heat generation and $\delta < 0$ represents heat absorption parameters, $\theta_w = T_w/T_\infty$: temperature difference parameter, $N_t = ((\rho c)_p D_T(T_W - T_\infty))/(\nu T_\infty\,(\rho c)_f)$: thermophoresis parameter $N_b = ((\rho c)_p D_B C_\infty)/(\nu\,(\rho c)_f)$; Brownian motion parameter, $Sc = \nu/D_B$: Schmidt number of mass.

The skin friction coefficient C_f, local Nusselt number Nu_x, local Sherwood number Sh and local density number of the motile microorganisms Nn_x are defined as

$$C_f = \frac{\tau_w}{\rho U_w^2}, \quad Nu_r = \frac{rq_w}{k(T_w - T_\infty)}, \quad \text{and} \quad Sh = \frac{rJ_w}{D_B(C_w - C_\infty)} \tag{11}$$

where

$$\tau_w = \mu_0\frac{\partial u}{\partial z}\left[1 + \Gamma^2\left(\frac{\partial u}{\partial z}\right)^2\right]^{(n-1)2}\Bigg|_{z=0},$$
$$q_w = -k\left(\frac{\partial T}{\partial z}\right) + (q_r)\Big|_{z=0};$$
$$J_w = -D_B\left(\frac{\partial C}{\partial z}\right)_{z=0} \tag{12}$$

$$C_f Re^{1/2} = \left\{f''(0)\left(1 + We^2 f''^2\right)\right\}^{(n-1)/2}\Big|_{\eta=0} \tag{13}$$

$$NuRe^{-1/2} = -\left(1 + \frac{4R}{3}\left\{1 + (\theta_w - 1)\theta(0)\right\}^3\right) \times \theta'(0) \tag{14}$$

$$Sh/\sqrt{Re} = -\phi'(0) \tag{15}$$

$Re = (ru_w)/\nu$: local Reynolds number.

4. RESULTS AND DISCUSSION

To conduct this study, we have set default values for the following parameters as suggested by several researchers such as $n = 0.5, We = 0.5, M = 0.5, Nt = 0.5, Nb = 0.5, R = 1.0, Sc = 2.0, Pr = 2.5, \theta_w = 1.1, Q = 0.03, Kn = 0.5, Me = 1.0$, $\text{slip}_1 = 0.5$, $\text{slip}_t = 0.5$, $\text{slip}_2 = 0.2$;

Keeping the view of the above values, we described the variation of pertinent parameters for various values, which are discussed graphically and in tabular form.

Figures 2–4 illustrate the f', θ and ϕ profiles for various values of the magnetic parameter M. Therefore, the effect of M is seen to decrease the f' and ϕ boundary layer while the θ is increased with the rise of the magnetic parameter. the speed curves show that the speed of transport decreases with the increasing distance (η) normal to the sheet. Altogether cases the speed vanishes at some large distance from the sheet (η). Figures 5–7, show

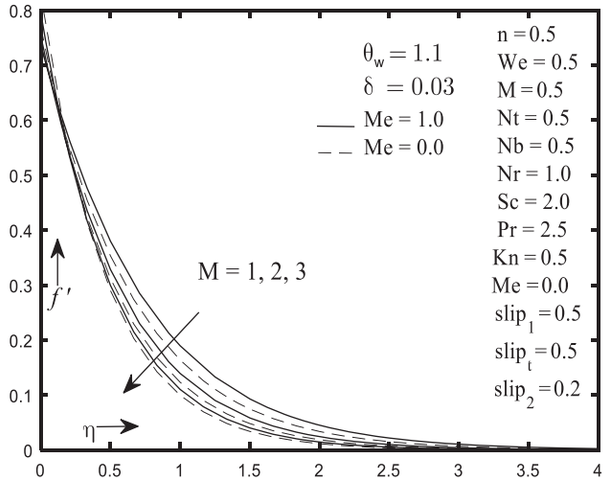

Fig. 2. Impact of *M* on velocity profile.

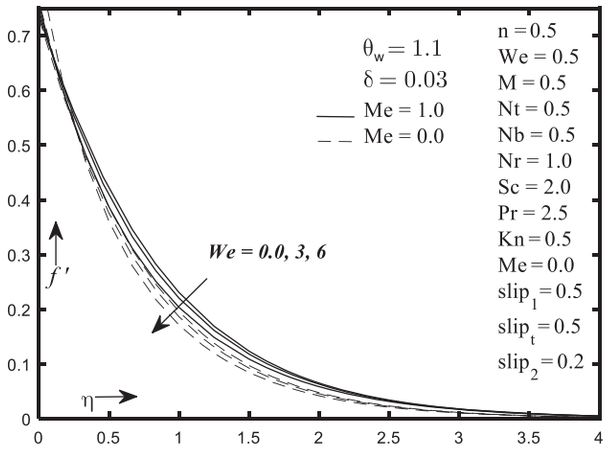

Fig. 5. Impact of *We* on velocity profile.

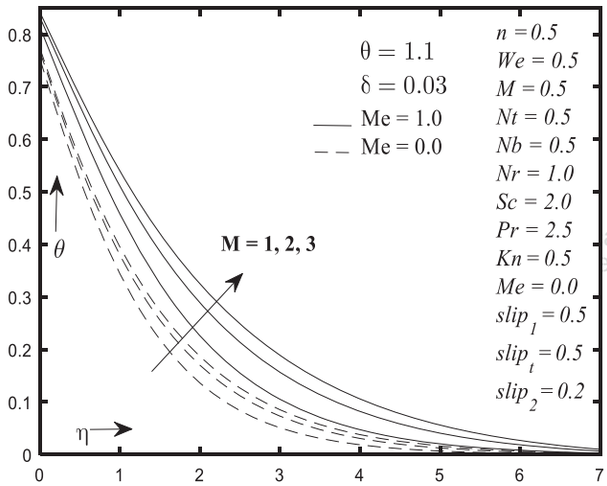

Fig. 3. Impact of *M* on temperature profile.

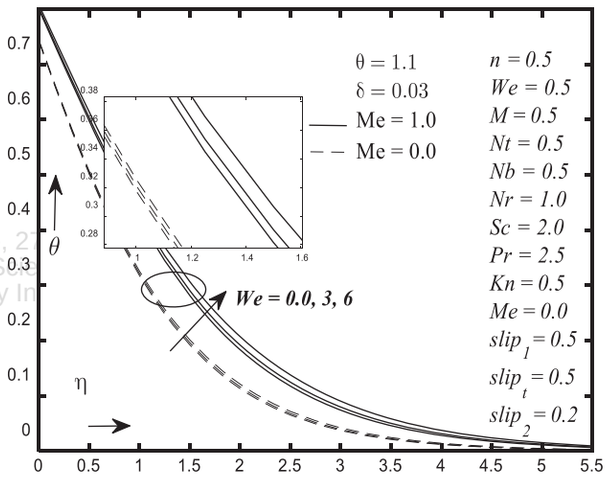

Fig. 6. Impact of *We* on temperature profile.

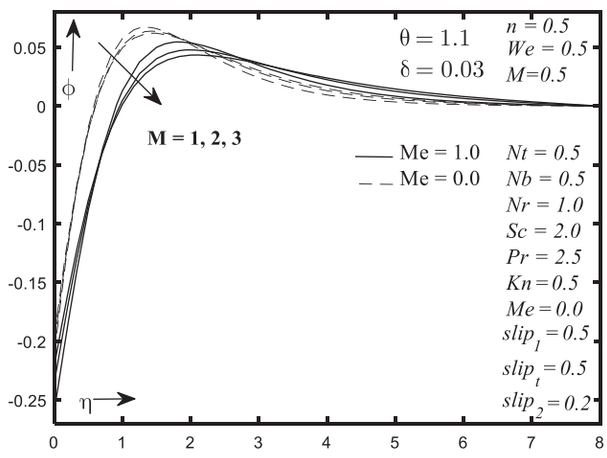

Fig. 4. Impact of *M* on mass profile.

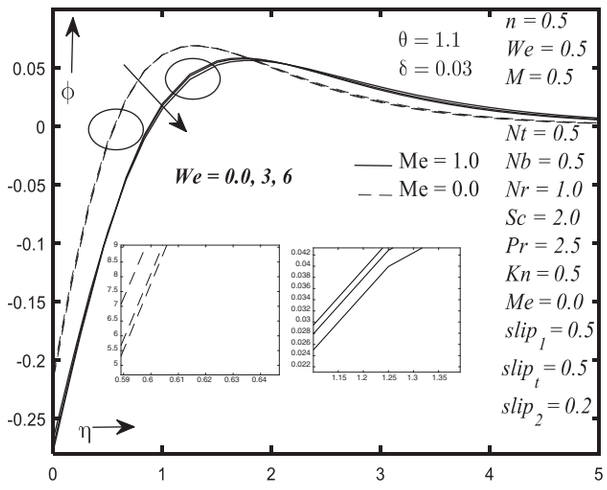

Fig. 7. Impact of *We* on mass profile.

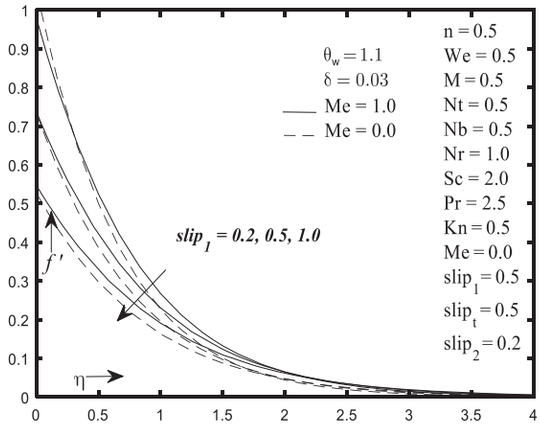

Fig. 8. Impact of $slip_1$ on velocity profile.

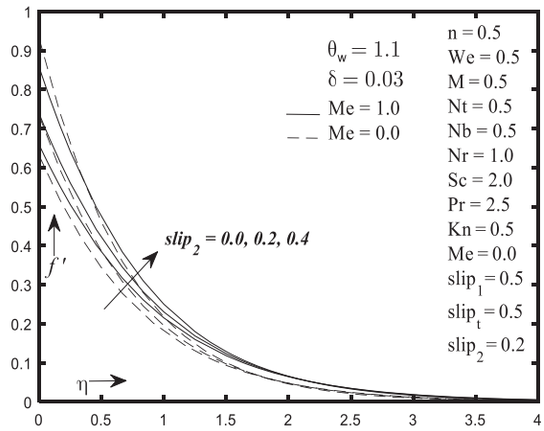

Fig. 11. Impact of $slip_2$ on velocity profile.

the effect of the Weissenberg number We on the evolution of fluid motion and behind the distribution of warmth and mass across the sheet as time evolves. Reduce in f' and ϕ boundary layer whereas the θ boundary layers increase when the Weissenberg number we effects intensify.

Figures 8–10 elucidate the effect of strength of first order velocity slip parameter ($slip_1$) on f', θ and ϕ profile fields. With an increment within the velocity slip first order parameter ($slip_1$) we've got perceived a fall within the momentum physical phenomenon and concentration profiles and a growth within the fluid temperature field. Figures 11–13 illustrate the effect of strength of velocity

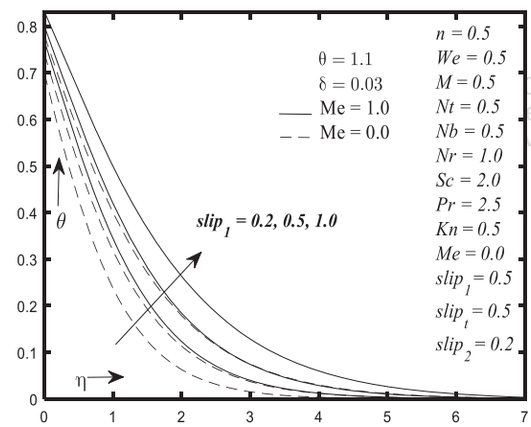

Fig. 9. Impact of $slip_1$ on temperature profile.

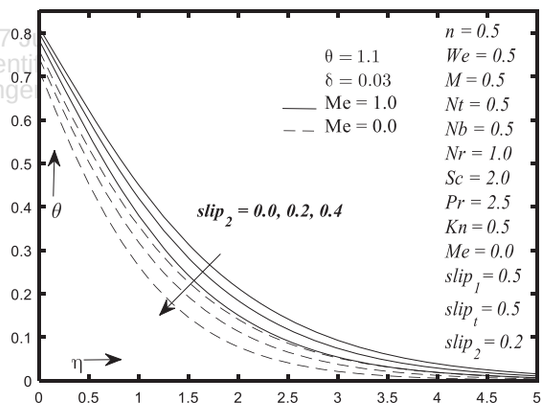

Fig. 12. Impact of $slip_1$ on temperature profile.

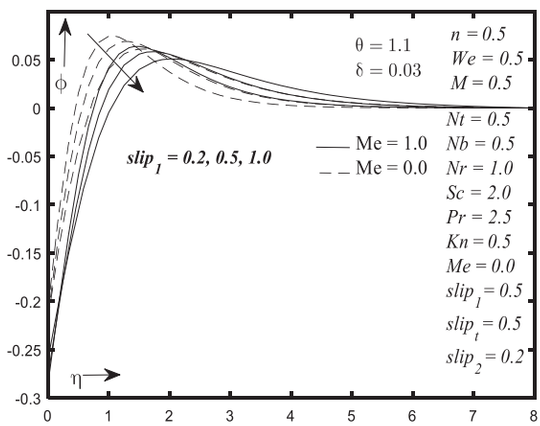

Fig. 10. Impact of $slip_1$ on mass profile.

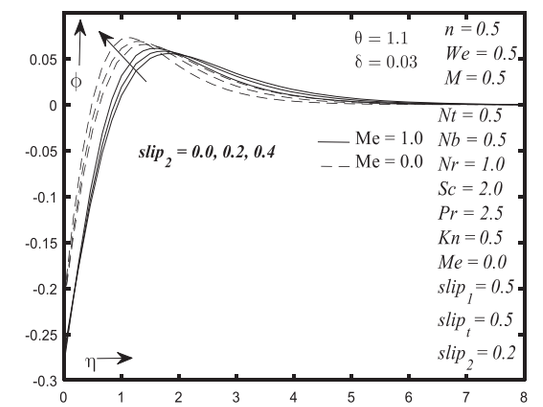

Fig. 13. Impact of $slip_2$ on mass profile.

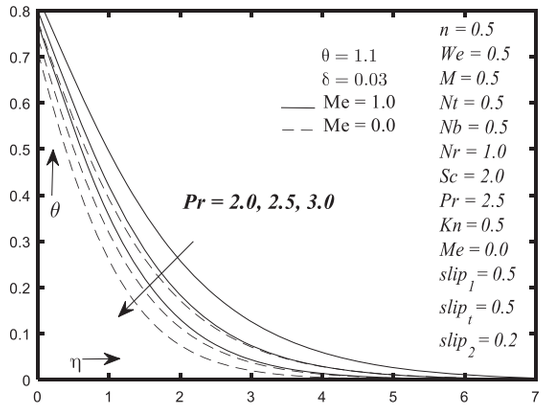

Fig. 14. Impact of *Pr* on temperature profile.

slip second order parameter ($slip_2$) on f', θ and ϕ profiles field. With an increment within the velocity slip second order parameter ($slip_2$) we've got perceived a lift within the momentum physical phenomenon and concentration profiles and a fall within the fluid temperature field profile.

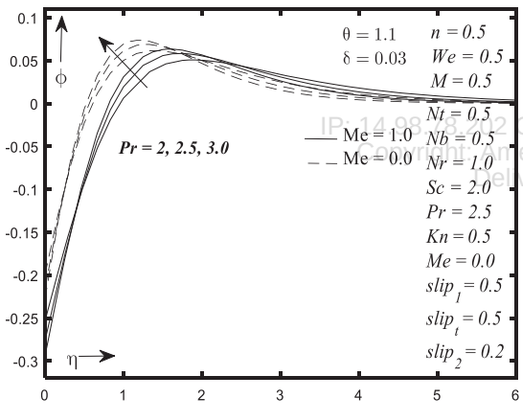

Fig. 15. Impact of *Pr* on mass profile.

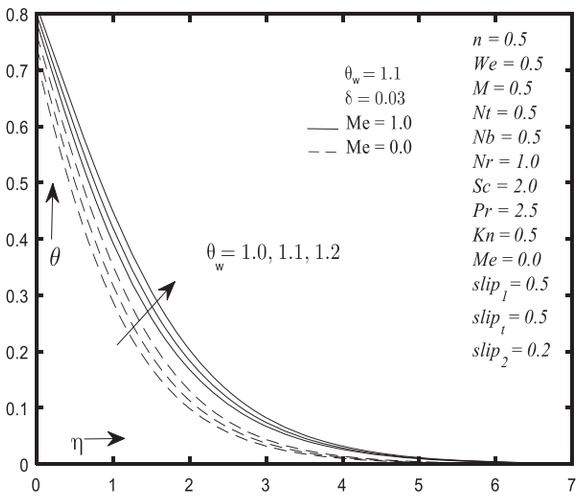

Fig. 16. Impact of θ_w on temperature profile.

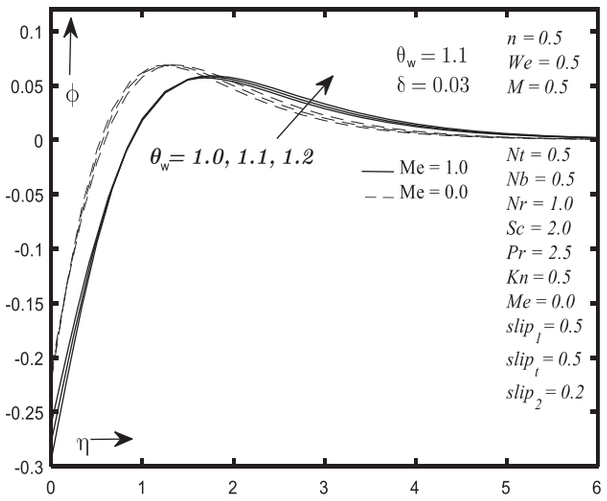

Fig. 17. Impact of θ_w on mass profile.

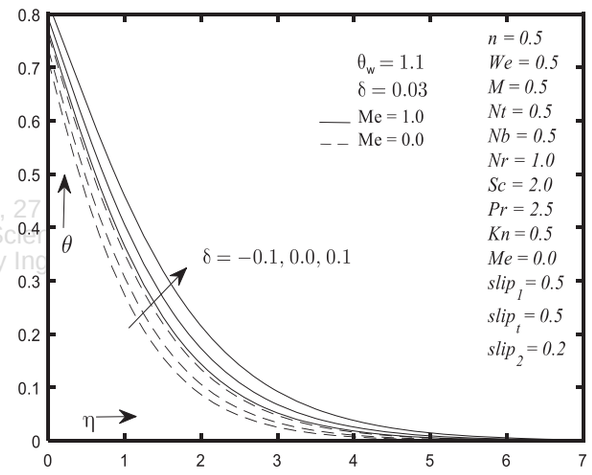

Fig. 18. Impact of δ on temperature profile.

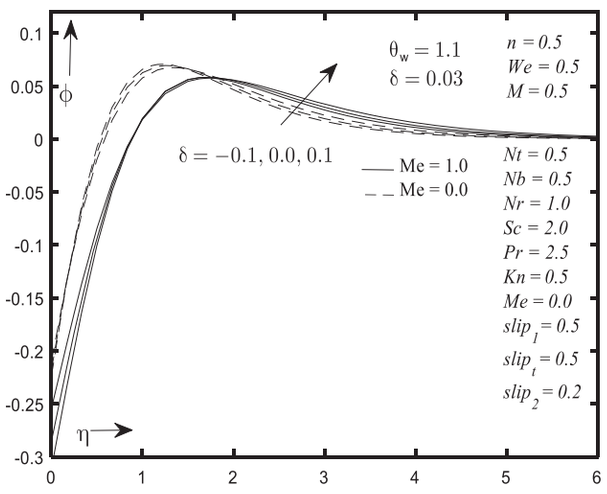

Fig. 19. Impact of δ on mass profile.

ARTICLE

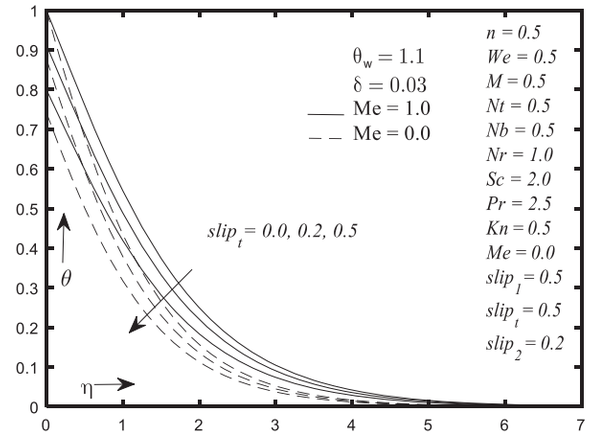

Fig. 20. Impact of slip$_t$ on temperature profile.

Figures 14–15 depict the effect of Pr on the fluid θ and ϕ profile fields. It's evident that for higher values of Pr number we noticed fall within the fluid temperature. An opposite result is observed in ϕ field. Figures 16–17

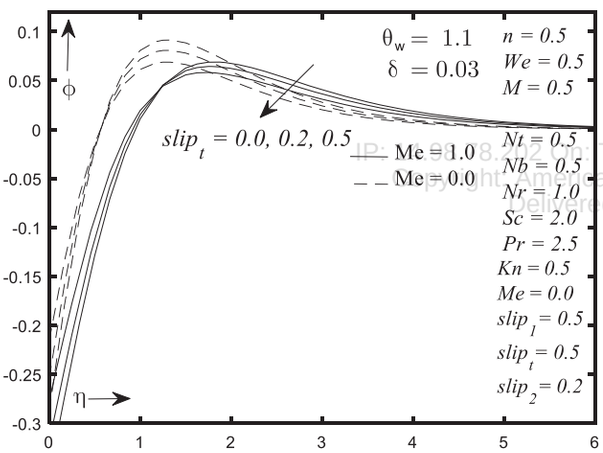

Fig. 21. Impact of slip$_t$ on mass profile.

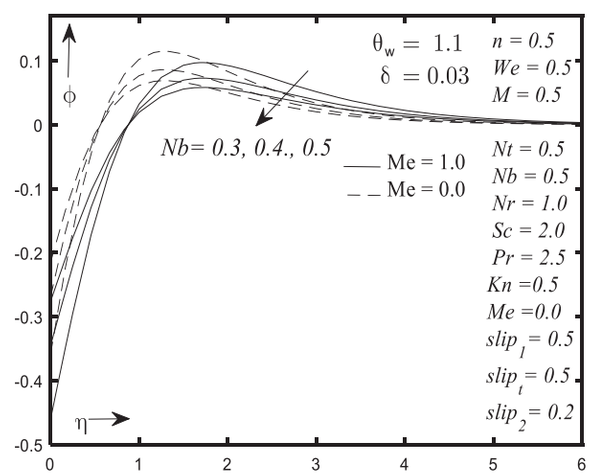

Fig. 22. Impact of *Nb* on mass profile.

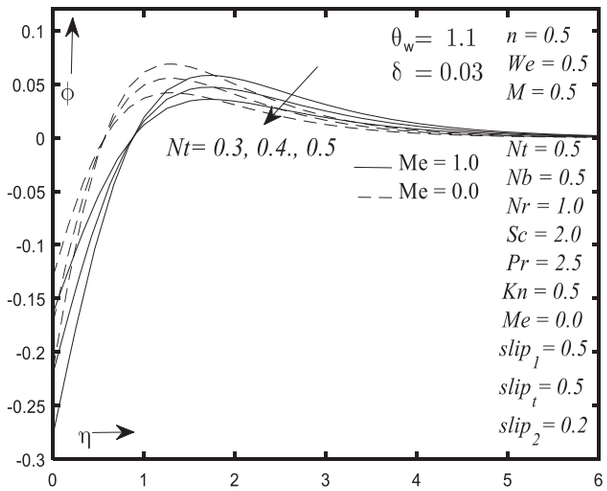

Fig. 23. Impact of *Nt* on mass profile.

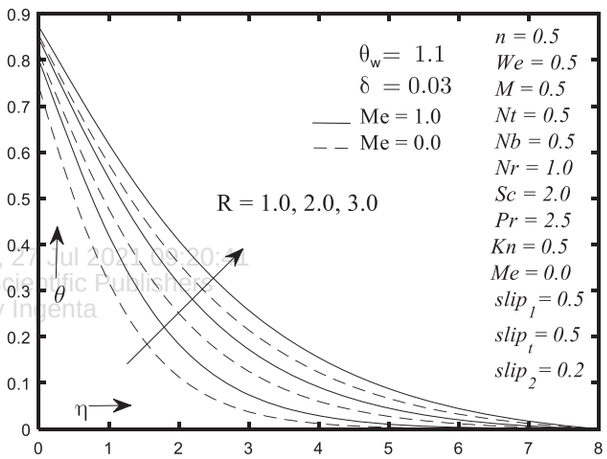

Fig. 24. Impact of *R* on temperature profile.

illustrate the temperature and concentration profiles for various values of temperature ratio parameter θ_w. It's evident that for higher values of θ_w parameter we noticed boosted within the fluid temperature and mass flux.

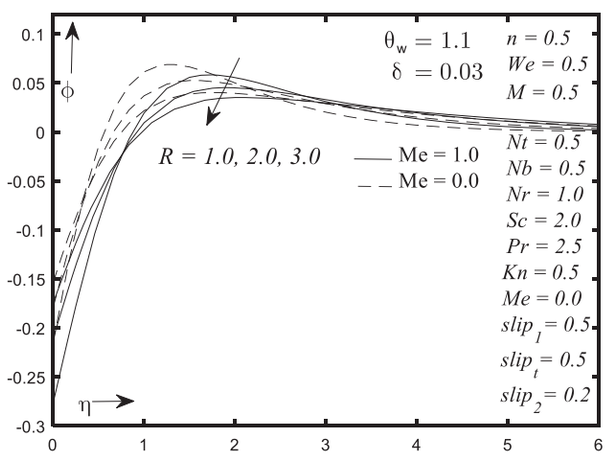

Fig. 25. Impact of *R* on mass profile.

Table I. The skin friction coefficient C_f, local Nusselt number Nu_x and local Sherwood number Sh are following physically parameter with melting surface.

M	We	Nb	$slip_1$	$slip_t$	$slip_2$	Melting $-C_f Re_x^{1/2}$	With out melting $-C_f Re_x^{1/2}$	Melting $-NuRe_x^{-1/2}$	With out melting $-NuRe_x^{-1/2}$	Melting $ShRe^{-1/2}$	With out melting $ShRe^{-1/2}$
1						0.8920	0.9907	1.0022	1.3122	0.3731	0.4937
2						1.1287	1.2358	0.9048	1.2377	0.3357	0.4645
3						1.3646	1.4942	0.8539	1.2082	0.3163	0.4529
	0					0.7885	0.8962	1.0740	1.3692	0.4008	0.5161
	3					0.5258	0.5878	1.0588	1.3627	0.3949	0.5136
	6					0.4103	0.4876	1.0315	1.3567	0.3844	0.5112
		0.3				0.7925	0.9036	1.0735	1.3691	0.6677	0.8602
		0.4				0.7925	0.9036	1.0735	1.3691	0.5008	0.6451
		0.5				0.7925	0.9036	1.0735	1.3691	0.4006	0.5161
			0.2			1.0784	1.3273	1.2362	1.5833	0.4639	0.6013
			0.5			0.7641	0.8626	1.0735	1.3691	0.4006	0.5161
			1.0			0.5294	0.5707	0.9096	1.1735	0.3376	0.4394
				0.0		0.7485	0.8626	1.3071	1.9198	0.4710	0.6919
				0.2		0.7551	0.8626	1.2051	1.6552	0.4410	0.6093
				0.5		0.7641	0.8626	1.0735	1.3691	0.4006	0.5161
					0.0	0.7751	0.9036	1.3071	1.9198	0.4710	0.6919
					0.2	0.7825	0.9036	1.2051	1.6552	0.4410	0.6093
					0.4	0.7925	0.9036	1.0735	1.3691	0.4006	0.5161

Table II. The skin friction coefficient C_f, local Nusselt number Nu_x and local Sherwood number Sh are following physically parameter with melting surface.

δ	Pr	Kn	Tw	Melting $-C_f Re_x^{1/2}$	With out melting $-C_f Re_x^{1/2}$	Melting $-NuRe_x^{-1/2}$	With out melting $-NuRe_x^{-1/2}$	Melting $ShRe^{-1/2}$	With out melting $ShRe^{-1/2}$
−0.1				0.7508	0.8626	1.2272	1.51517	0.4604	0.57407
0.0				0.7607	0.8626	1.1128	1.4064	0.4158	0.5308
0.1				0.7732	0.8626	0.9690	1.2702	0.3603	0.4772
	2.0			0.7583	0.8626	0.9192	1.1879	0.3412	0.4450
	2.5			0.7641	0.8626	1.0735	1.3691	0.4006	0.5161
	3.0			0.7689	0.8626	1.2145	1.5290	0.4554	0.5796
		0.0		0.7625	0.8626	1.0922	1.3757	0.4079	0.5187
		0.2		0.7632	0.8626	1.0840	1.3743	0.4047	0.5181
		0.5		0.7641	0.8626	1.0735	1.3691	0.4006	0.5161
			1.0	0.7577	0.8626	1.0014	1.3081	0.4292	0.5606
			1.1	0.7641	0.8626	1.0735	1.3691	0.4006	0.5161
			1.2	0.7707	0.8626	1.1505	1.4341	0.4712	0.3715

Figures 18–19 illustrate the θ and ϕ profiles for various values of warmth source parameter δ. It's evident that for higher values of δ parameter we noticed boosted within the fluid temperature and mass flux. Figures 20–21 illustrate the effect of strength of temperature slip parameter ($slip_t$) on θ and ϕ field. With an increment within the ($slip_t$) parameter we've got perceived a fall within the fluid θ and ϕ profile fields. The effect of Nb and Nt on the ϕ profile is shown in Figures 22–23. From the sooner graphical results, we've got noticed that the thickness of the concentration boundary layers reduces with the rise within the rate of Nb and Nt. Figures 24–25 show the impact of R parameters on profile. From these graphs, it's clear that the surface temperature increases with increases within the value of the R parameter. Generally, increasing values of R, the mean coefficient decreases, and this end in rise to the divergence of radiative heat flux. Hence, the speed of radiative heat transferred to the fluid increase, so the fluid temperature increases.

Tables I and II shows the effect of skin friction coefficient, Nusselt Number, and native Sherwood number for the subsequent physical parameters. Tables III and IV

Table III. Comparison of $f''(0)$ for different values M in the absence of the parameters $n = 0.5$, $We = slip_1 = slip_2 = Me = 0$.

M	Makinde et al.[25]	Azam et al.[26]	Ramzan et al.[27]	Present study
0.0	−1.17372	−1.17372	−1.173720	−1.173723741
0.5	−1.36581	−1.36581	−1.365814	−1.365812821
1	−1.53571	−1.53571	−1.535709	−1.535706485
2	−1.83049	−1.83049	−1.830490	−1.830479953
3	−2.08484	−2.08485	−2.084846	−2.084830040

Table IV. Comparison of $-f''(0)$ for different values M, We and n in the absence of the parameters $S = R = \text{slip}_1 = \text{slip}_2 = \text{slip}_t = \delta = 0.0$; $\theta_w = 1$, $Pr = 2.5$.

M	We	n	Ramzan et al.[27]	Present study
0.5	0.05	0.5	1.3653398	1.365998701
1			1.5350602	1.535975266
1.5			1.6884948	1.689691502
2			1.8294374	1.830942819
0.5	0.05	1	1.3653398	1.365324607
	2.0		1.0492851	1.049276808
	4.0		0.85467461	0.854673610
	6.0		0.75112133	0.751120290
0.5	0.05	0.5	1.3653398	1.364410274
		1	1.3658144	1.365812557
		1.5	1.3662882	1.366843336
		2	1.3667611	1.367501566

compression present results with existing literature for various parameters.

5. CONCLUSION

In this article we've investigated is pagination to explore the numerical solution of physical phenomenon flow for MHD Carreau nano-fluid, heat and mass transport to deliberate the combine impact of second order velocity slip with zero mass flux over a malting radial surface with. The impact of non-liner thermal radiation, heat source and temperature jump effects also are taken under consideration. And also consider the cross-diffusion effect on temperature and mass equations. The impact of pertinent flow parameters like, first and second order velocity slip parameter, temperature jump, magnetic parameter, heat source, radiation parameter, melting surface parameter, temperature ratio parameter on dimensionless velocity, temperature and concentration profiles are displayed graphically while local skin friction, Nusselt number and Sherwood number are demonstrated within the sort of Tables. The obtained results confirm that a wonderful agreement is achieved with those available in open literature. It's found that skin friction increases within the presence of first and second order slip parameter whereas opposite behavior in noted for Nusselt number.

- For different values of the magnetic parameter M. Therefore, the effect of M is seen to decrease the f' and ϕ boundary layer while the θ is increased with the rise of the magnetic parameter.
- Weissenberg number We on the evolution of fluid motion and succeeding the distribution of warmth and mass across the sheet as time evolves. Reduction in f' and ϕ boundary layer, whereas the θ boundary layers increase when the Weissenberg number We effects intensify.
- Velocity slip first order parameter (slip_1) on f', θ and ϕ profile fields. With an increment within the velocity slip first order parameter (slip_1) we've perceived a fall within the momentum physical phenomenon and concentration profiles and a growth within the fluid temperature field.
- Velocity slip second order parameter (slip_2) on f', θ and ϕ profiles field. With an increment within the velocity slip second order parameter (slip_2) we've perceived a lift within the momentum physical phenomenon and concentration profiles and a fall within the fluid temperature field profile.
- The effect of Pr on the fluid θ and ϕ profile fields. It's evident that for higher values of Pr number we noticed fall within the fluid temperature. An opposite result are observed for ϕ field.
- It is clear that for higher values of θ_w parameter we noticed boosted within the fluid temperature and mass flux.
- It is obvious that for higher values of δ parameter we noticed boosted within the fluid temperature and mass flux.
- The effect of strength of temperature slip parameter (slip_t) on temperature and con-centration field. With an increment within the temperature slip parameter (slip_t) we've got perceived a fall within the fluid temperature and concentration profile fields.
- The thickness of the concentration boundary layers reduces with the rise within the rate of Nb and Nt.
- It is obvious that the surface temperature increases with increases within the value of the R parameter.

Conflict of Interests

The authors declare that there is no conflict of interests regarding the publication of this paper.

References and Notes

1. M. Khan, M. Azam, and A. S. Alshomrani, *Int. J. Heat Mass Tran.* 110, 437 (**2017**).
2. M. Azam, M. Khan, and A. S. Alshomrani, *Int. J. Mech. Sci.* 130, 64 (**2017**).
3. M. Khan and M. Azam, *J. Mol. Liq.* 225, 554 (**2017**).
4. M. Khan, M. Hussain, and M. Azam, *J. Magn. Magn. Mater.* 412, 63 (**2016**).
5. M. Khan, M. Azam, and A. S. Alshomrani, *Results Phys.* 7, 2671 (**2017**).
6. T. Hayat, I. Ullah, B. Ahmad, and A. Alsaedi, *Results Phys.* 7, 715 (**2017**).
7. T. Hayat, M. Waqas, S. A. Shehzad, and A. Alsaedi, *Pramana.* 86, 3 (**2016**).
8. M. Waqas, I. Khan, T. Hayat, and A. Alsaedi, *Comput. Method Appl. M* 324, 640 (**2017**).
9. C. Sulochana, G. P. Ashwinkumar, and N. Sandeep, *Alexand. Eng. J.* 55, 1151 (**2016**).
10. M. Ramzan, J. D. Chung, and N. Ullah, *Results. Phys.* 7, 3557 (**2017**).
11. M. Ramzan, J. D. Chung, and N. Ullah, *Int. J. Mech. Sci.* 130, 31 (**2017**).
12. M. Ramzan, M. Bilal, S. Kanwal, and J. D. Chung, *Commun. Theor. Phys.* 67, 723 (**2017**).
13. M. M. Rahman and I. A. Eltayeb, *Int. J. Therm. Sci.* 50, 468 (**2011**).
14. M. M. Rahman and I. A. Eltayeb, *Meccanica.* 48, 601 (**2013**).
15. H. Upreti, A. K. Pandey, and M. Kumar, *Alexand. Eng. J.* 57, 1839 (**2018**).

16. M. Turkyilmazoglu, *Int. J. Heat Mass Tran.* 55, 6959 (**2012**).
17. M. Goyal and R. Bhargava, *Appl. Nanosci.* 4, 761 (**2014**).
18. N. A. Khan, S. Khan, and F. Riaz, *Math. Sci. Lett.* 3, 199 (**2014**).
19. S. Jain and R. Choudhary, *Global and Stochastic Analysis* SI, 75 (**2017**).
20. S. Jain and R. Choudhary *Procedia Engineering* 127, 1203 (**2015**).
21. S. Jain and A. Parmar, *Global and Stochastic Analysis* SI, 41 (**2017**).
22. M. M. Rahman, *Can. J. Chem. Eng.* 90, 1631 (**2012**).
23. A. M. Megahed, *Eur. Phys. J. Plus* 130, 81 (**2015**).
24. R. S. R. Gorla, M. R. Krishnamurthya, B. C. Prasannakumara, and B. J. Gireesha, *Engineering Science and Technology, An International Journal* 19, 53 (**2016**).
25. O. D. Makinde, F. Mabood, W. A. Khan, and M. S. Tshehla, *J. Mol Liq.* 219, 624 (**2016**).
26. M. Azam, M. Khan, and A. S. Alshomrani, *Results Phys.* 7, 2671 (**2017**).
27. M. Ramzan, D. Lu, Noor ul Huda, J. D. Chung, and U. Farooq, *Sci. Rep.* 8, 3709 (**2018**).
28. S. U. S. Choi, *ASME Int. Mech. Eng.* 66, 99 (**1995**).
29. W. Muhammad, J. Shagufta, H. M. I. K. Tasawar, and A. Ahmed, *J. Magn. Magn. Mater.* 485, 197 (**2019**).
30. M. Irfan, W. A. Khan, M. Khan, and M. M. Gulzar, *J. Phys. Chem. Solids* 125, 141 (**2018**).
31. M. R. Eid, K. L. Mahny, A. Dar, and T. Muhammad, *Physica A: Statistical Mechanics and Its Applications* 540, 123063 (**2020**).
32. M. V. Krishna, N. A. Ahamad, and A. J. Chamkha, *Alexand. Eng. J.* 60, 845 (**2021**).
33. M. V. Krishna and A. J. Chamkha, *International Communications in Heat and Mass Transfer* 113, 104494 (**2020**).
34. M. V. Krishna, N. A. Ahamad, and A. J. Chamkha, *Alexand. Eng. J.* 59, 565 (**2020**).
35. M. V. Krishna and A. J. Chamkha, *Results Phys.* 15, 102652 (**2019**).
36. A. S. Dogonchia, S. R. Mishrab, N. Kumar, A. J. Chamkh, and H. Alhumade, *Journal of the Taiwan Institute of Chemical Engineers* (**2021**), in press.
37. M. S. Sadeghia, A. S. Dogonchi, M. Godrat, A. J. Chamkha, H. Alhumad, and N. Karimih, *Journal of the Taiwan Institute of Chemical Engineers* (**2021**), in press.
38. M. S. Sadeghi, N. Anadalibkhah, and R. Ghasemiasl, *J. Therm. Anal. Calorim.* (**2020**).
39. M. S. Sadeghia, T. Tayebib, A. S. Dogonchi, M. K. Nayak, and M. Waqas, *International Communications in Heat and Mass Transfer* 120, 104951 (**2021**).
40. A. S. Dogonchi, T. Tayebi, and A. J. Chamkha, *J. Therm. Anal. Calorim.* 139, 661 (**2020**).
41. A. S. Dogonchi, T. Armaghani, and A. J. Chamkha, *Arab. J. Sci. Eng.* 44, 7919 (**2019**).
42. M. A. Ismael, T. Armaghani, and A. J. Chamkh, *Journal of the Taiwan Institute of Chemical Engineers* 59, 138 (**2016**).
43. A. S. Dogonchi, A. J. Chamkha, S. M. Seyyedi, M. H. Tilehnoee, and D. D. Ganji, *J. Appl. Comput. Mech.* 5, 717 (**2019**).
44. H. S. Takhar, A. J. Chamkha, and G. Nath, *Heat Mass Transf.* 39, 297 (**2003**).
45. A. J. Chamkha and A. A. Khaled, *International Journal of Numerical Methods for Heat and Fluid Flow* 10, 94 (**2000**).
46. S. Parvina and A. J. Chamkha, *International Communications in Heat and Mass Transfer* 54, 8 (**2014**).
47. M. Ghalambaz, A. Doostani, and E. Izadpanahi, *J. Therm. Anal. Calorim.* 139, 2321 (**2020**).
48. B. Kumara, G. S. Setha, R. Nandkeolyar, and A. J. Chamkh, *International Journal of Thermal Sciences* 146, 106101 (**2019**).
49. M. V. Krishna and A. J. Chamkh *Results Phys.* 15, 102652 (**2019**).
50. A. S. Dogonchi, T. T. N. Karim, A. J. Chamkh, and H. Alhumad, *Journal of the Taiwan Institute of Chemical Engineers* (**2021**), in press, https://www.sciencedirect.com/science/article/abs/pii/S1876107021002042.
51. M. V. Krishna, M. G. Reddy, and A. J. Chamkh, *Int. Jour. of Fluid Mech. Res.* 45, 1 (**2019**).
52. M. V. Krishna, M. G. Reddy, and A. J. Chamkh, *Journal of Porous Media* 24, 81 (**2021**).
53. M. V. Krishna and A. J. Chamkh, *International Communications in Heat and Mass Transfer* 113, 104494 (**2020**).
54. M. V. Krishna and A. J. Chamkh, *Results Phys.* 15, 102652 (**2019**).
55. M. V. Krishna and B. V. A. J. Swarnalathamma, *Journal of Ocean Engineering and Science* 4, 263 (**2019**).
56. M. V. Krishna and A. J. Chamkh, *Journal of Porous Media* 22, 209 (**2019**).
57. M. V. Krishna and A. J. Chamkh, *Journal of Egyptian Mathematical Society* 28, 1 (**2020**).
58. M. V. Krishna and A. J. Chamkh *Ain Shams Engineering Journal* 11, 1 (**2020**).
59. M. V. Krishna, N. A. Ahamad, and A. J. Chamkh, *Ain Shams Engineering Journal* 11, 1 (**2021**).
60. M. V. Krishna, N. A. Ahamad, and A. J. Chamkh, *Alexand. Eng. J.* 60, 845 (**2021**).
61. M. V. Krishna and A. J. Chamkh, *Special Topics and Reviews in Porous Media: An International Journal* 10, 245 (**2019**).
62. M. V. Krishna and A. J. Chamkh, *AIP Conference Proceedings* 1728, 020461 (**2016**).